Ultrafast acoustic resonance spectroscopy of gold nanostructures: Towards a generation of tunable transverse waves

A. Amziane,[1] L. Belliard,[1,*] F. Decremps,[2] and B. Perrin[1]

[1]*Institut des NanoSciences de Paris, UMR7588 CNRS, Université Pierre et Marie Curie, 140 rue de Lourmel, F-75015 Paris, France*

[2]*Institut de Minéralogie et Physique des Milieux Condensés, Université Pierre et Marie Curie-Paris 6, CNRS UMR 7590, 140 rue de Lourmel, F-75015 Paris, France*

(Received 30 July 2010; revised manuscript received 25 October 2010; published 18 January 2011)

Femtosecond pump-probe experiments have been carried out on circular single gold nanostructures lithographed on a silicon substrate with diameters ranging from 1.1 down to 0.3 μm and thicknesses of 175 down to 55 nm. Using three-dimensional finite-element simulations coupled to the specific detection rule of interferometric measurements, we illustrate the effect of intrinsic parameters such as the size and the boundary conditions on the vibrational spectrum. The possibility of using these artificial nanostructures for acoustic transduction in the underlying substrate is investigated. Gold nanostructures are good candidates to generate monochromatic transverse bulk waves in the gigahertz frequency range, with frequency tuned by the dot size.

DOI: 10.1103/PhysRevB.83.014102 PACS number(s): 62.25.Fg, 62.25.Jk

I. INTRODUCTION

The optoacoustical response of single submicronic structures is currently drawing a great deal of interest for fundamental and technological applications. The surface-plasmon resonance, related to size reduction in the nanometer scale, is one of the most illustrated phenomena.[1] Vibrating mechanical components with high-quality factors are intensively studied for bandpass filters in radio applications.[2]

Picosecond ultrasonic measurements with high spatial resolution are well adapted to study the vibrational landscape of such individual structures.[3] Indeed, local investigations on single resonators here are free from the averaging process. In 1984, Maris introduced the picosecond ultrasonics technique, which uses femtosecond laser pulses to generate and detect acoustic waves.[4] One of the advantages of this powerful technique is the large frequency domain of the generated acoustic waves, mainly imposed by the optical properties of the materials. In this way, a frequency range from 100 GHz up to 1 THz is now achieved, overcoming by three orders of magnitude the bandwidth limitations associated with standard piezoelectric sensors. These ultrashort acoustic waves have been used to investigate acoustic properties in various systems, such as thin films,[5] superlattices,[6–8] isolated dots.[9–11] or buckling structures.[12]

Although mostly longitudinal waves are generated in such experiments, shear wave generation and detection have also been considered in picosecond ultrasonics. The propagation of surface acoustic waves, induced by micrometer laser spot excitation,[13] has been performed in various systems.[14] Recently, the acoustic diffraction effect in a thin layer has been investigated, and it was revealed that both bulk and surface waves could be generated.[15] The conversion mode at the interface between isotropic film and anisotropic substrate[16] or laser generation in a tilted anisotropic system[17] have also been investigated as an alternative approach to generate bulk shear waves. Different mechanisms of shear wave generation in picosecond ultrasonics could be found in Refs. 18–20. Here we emphasize that the frequency of the shear waves is, however, strongly correlated to the sample elasticity and the laser spot size.

In the past, periodic confined systems have been considered to be an efficient way to create surface waves with tunable frequency.[21,22] Recently, longitudinal waves generated by gold nanoparticles in the surrounding matrix have been demonstrated,[11] but the emission of bulk transverse waves by a local resonator in the gigahertz range has not yet been reported. As a consequence, a transducer able to emit a tunable acoustic pulse with a transversal polarization is still needed.

In this paper, time-resolved picosecond acoustic measurements on a series of single gold lithographed nanostructures with thickness ranging from 45 up to 175 nm and a diameter of 1.1 μm down to 0.3 are presented. In the first part, a better understanding of the experimental vibrational spectrum has been achieved mixing three-dimensional (3D) finite-element simulations and specific experimental detection rules. The last part is devoted to the large potential of such lithographed structures to act as a tunable bulk shear wave's transducer. Acoustic transmission across a thick silicon wafer of bulk shear waves with different frequencies is demonstrated and related to the relaxation of a given specific mode of vibration.

II. EXPERIMENTAL DETAILS AND SAMPLE DESCRIPTION

A. Sample preparation

A standard lift-off process is used to create a pattern of circular dots with diameter ranging from 1.1 down to 0.3 μm. Until 0.5 μm, direct uv laser lithography (for printing the pattern in a negative resin) gives a satisfactory optical resolution. For a smaller size, electron-beam lithography with usual *PMMA* photosensitive resins is mandatory. Figure 1 shows a typical pattern of circular dots (with a well-defined cylindrical shape) on a 160-μm-thick (100) silicon wafer. A small fluctuation of the dot side has been observed with an edge roughness estimated at 10 nm. The gold nanostructures have been organized into a 2D square lattice for experimental

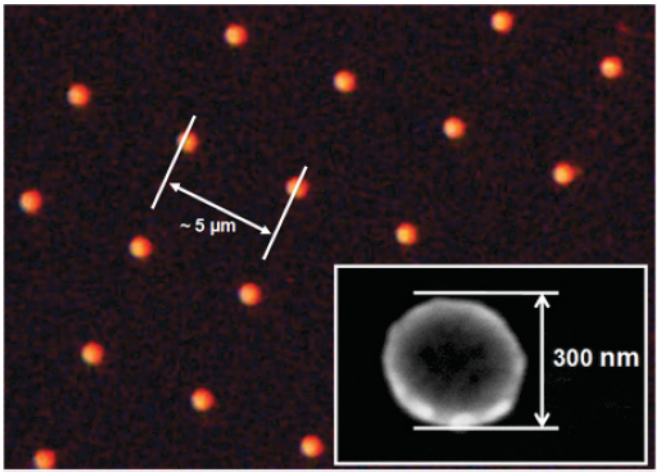

FIG. 1. (Color online) Regular dot lattice used in this work. The distance between two structures, far greater than the laser size, allows measurements on individual gold dots. Inset: Scanning electron microscopy picture of a 0.3-μm-diam gold nanostructure.

convenience. The lattice parameter has been chosen larger than the pump-and-probe spot diameter to realize individual excitation and detection of dot vibrations. In the present work, the chromium layer buffer, usually used to obtain a good gold adhesion, has been suppressed. Then possible variations of the elastic properties such as the Young modulus or the Poisson ratio could exist. This choice has been motivated to reduce the substrate influence on the dot's individual mode of vibration (cf. Sec. III A).

B. Picosecond ultrasonics

A femtosecond laser pulse (the pump beam), absorbed at the sample surface, generates acoustic waves by thermal expansion, which propagate inside the material. The real and imaginary parts of the relative change of surface reflectivity $[\Delta r(t)/r_0]$ induced by the strain field can be measured either by reflectivity[23–25] or interferometric measurements,[26–29] using a time-delayed laser pulse (commonly called the probe beam). In a 1D photoacoustic model, the change of sample reflectivity induced by an acoustic wave is given by the following equation:

$$\frac{\Delta r\,(t)}{r_0} = ik_0\frac{4n}{1-n^2}\frac{\partial n}{\partial \eta}\int_0^\infty \eta\,(z,t)\exp\left(2ik_0 nz\right)dz + 2ik_0 u\,(0,t) \quad (1)$$

with n the optical index, $\partial n/\partial\eta$ the photoelastic coefficient, $u\,(0,t)$ the surface sample displacement, and $\eta\,(z,t) = \partial u_z/\partial z$, with u the displacement field and z the coordinate perpendicular to the surface.

Briefly, we use a mode-locked Ti:sapphire (MAI-TAI Spectra) laser source operating at 800 nm, with a repetition rate around 79.8 MHz. The pulse time width is less than 100 fs at the laser output. The pump beam is modulated at 1.8 MHz to perform synchronous detection on the sample reflectivity.

The front side configuration [described in Fig. 2(a)] is used to study the vibrational response of a single nanostructure. The pump and probe are focused by the same objective with a numerical aperture equal to 0.9. The probe spot diameter d is estimated to be 0.75 μm at $1/e^2$ on the Gaussian intensity profile. The sample, fixed on a piezoelectric stage, can be moved in the focalization plane to select a single dot. In this geometry, scattered light coming from the pump strongly affects the lock-in detection. To avoid such a parasite signal, a two-color experiment is performed by doubling the pump frequency ($\lambda = 400$ nm) with a nonlinear crystal. Then, a dichroic filter located in front of the diode system suppresses the pump diffusion. Finally, acoustic measurements using a stabilized Michelson interferometer have been recorded. More experimental details about this front side configuration could be found elsewhere.[30,31]

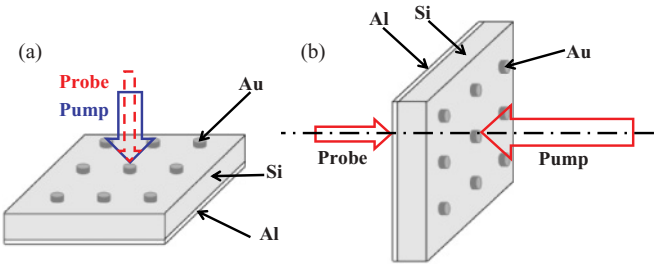

FIG. 2. (Color online) (a) Front side configuration. The pump and probe are focused on a single dot using the same objective. (b) Back side configuration. The probe and the pump beams are focused on both sides of the sample. The sample can be moved to excite a single dot with the pump beam.

The back side configuration [Fig. 2(b)] has been used to investigate the transduction properties of the lithographed dots. The pump is focused here on a single dot into a 3-μm-spot size. After propagation through the silicon substrate, the acoustic response is recorded through the change of the probe reflectivity on an aluminum layer (100 nm) deposited at the opposite side. The probe objective is fixed on a second piezoelectric stage, which allows us to locate the pump epicenter through an acoustic field mapping. More experimental details about this back side configuration are described in Refs. 8 and 32.

The probe and pump powers used to perform the acoustic measurements have been measured at 3 and 1 mW, respectively. Owing to the laser modulation, the pulse energy E_L is approximately 37.6 pJ for the probe and 12.5 pJ for the pump. The laser power density for a spot of diameter d is defined by

$$I = \frac{8E_L}{\tau_L \pi d^2} = I_{\text{pump}} + I_{\text{probe}} \quad (2)$$

with τ_l the laser pulse duration. Taking into account the gold reflectance at 400 and 800 nm,[33] and a laser spot diameter of 0.75 μm, the total power density deposited on a gold dot is estimated at 38 GW/cm^2. This value is slightly higher than the theoretical ablation thresholds I of about 22.3 GW/cm^2,[34] nevertheless no damage on the dots has been observed during the measurements.

III. RESULTS AND DISCUSSION

A. Gold nanostructure vibration

The time evolution of $\Delta r(t)/r_0$ for a dot is mainly dominated by oscillations with a spectrum determined by its shape,

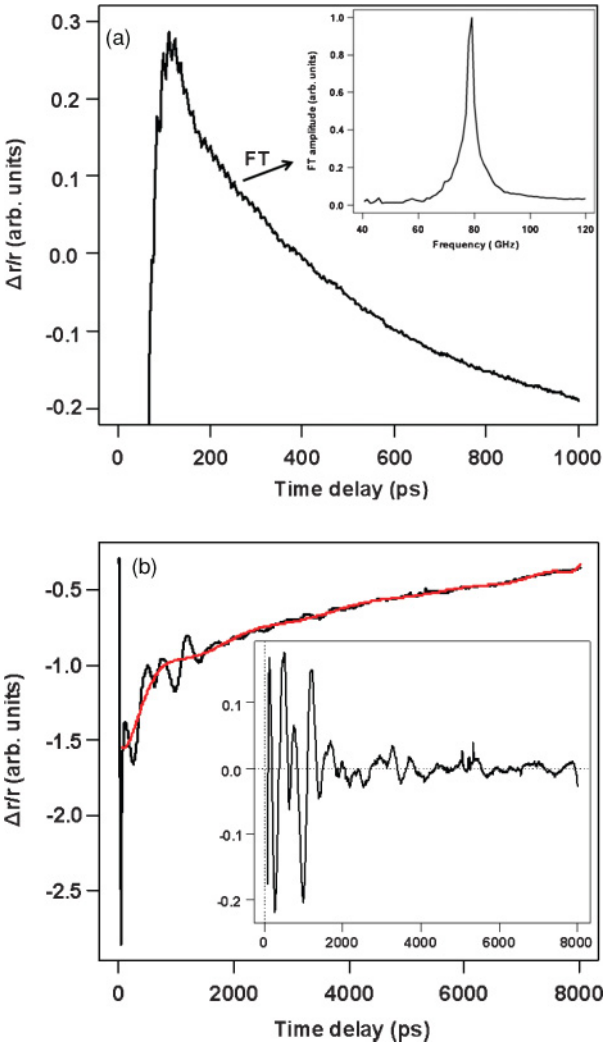

FIG. 3. (Color online) (a) Interferometric time-resolved signal recorded on the silicon substrate. Brillouin oscillations are clearly visible superimposed on a decreasing photothermal background. Inset: The FFT amplitude reveals a monochromatic response. (b) Signal obtained on a gold dot with 0.9-μm diam and 55-nm thickness. Inset: Signal where the photothermal background has been removed to clearly isolate the oscillatory dot response.

the elastic properties, and by the boundary conditions at the interface with the substrate.

In a first step, the acoustical response of a single gold dot with 0.9-μm diam and 55-nm thickness has been measured. Figure 3 shows the imaginary part of the optical reflection of a gold dot compared with the one recorded on the silicon substrate (between the dots). Superimposed to the thermal background, the acoustic signal of the substrate [Fig. 3(a)] is characterized by typical oscillations, so-called Brillouin oscillations, resulting from interferences between light reflection by the surface and the acoustic pulse propagating into the semitransparent silicon substrate. For a normal incidence, a frequency $F = 2nV\cos(\theta)/\lambda = 77.9$ GHz (with n the optical index, V the sound velocity, λ the wavelength of the probe and θ the incident light angle) is expected, in excellent agreement with our experimental findings, namely 78.0 GHz.

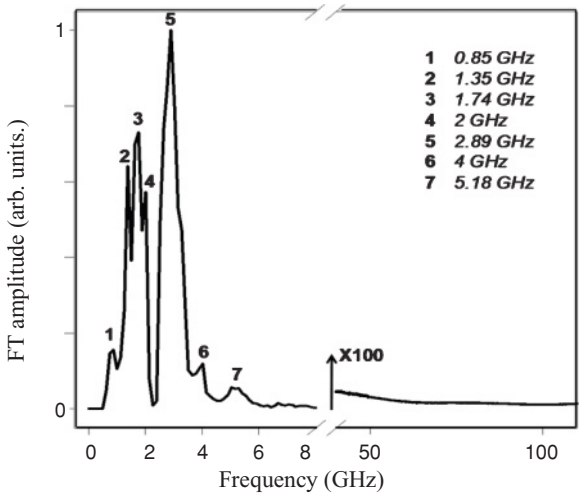

FIG. 4. FFT spectra of the signal shown in Fig. 3(b). The frequencies of vibrational modes are labeled from 1 to 7. Note that no Brillouin component is detected around 78 GHz in spite of a magnification factor of 100.

However, the signal recorded onto a single gold dot exhibits quite a different acoustic feature [Fig. 3(b)]. Following the electronic response, large oscillations are observed over an extended time scale, up to 6 ns. No Brillouin oscillations can be observed in the fast Fourier transform (FFT) signal, which is consistent with the fact that no probe light reaches the silicon substrate due to a probe size (0.75 μm) smaller than the dot diameter. As shown in Fig. 4, the acoustic response of the gold dot presents several characteristic frequencies ranging from 0.85 to 5.2 GHz.

This set of frequencies corresponds to the vibrational modes, characteristic of the object (the dot) and the boundary conditions. An assignment of each vibrational mode can be obtained through a vibroacoustic modeling work based on 3D finite-element simulations. This technique is well adapted to our case, being able to account for different boundary conditions over the whole surface of the studied dot. Hypothesis and technical details of our calculations can be resumed as follows. The structure is decomposed into simple elements with mechanical behavior reduced to the motion of the mesh points. The dots have been meshed with a standard tetrahedral parabolic with an average edge of 25 and 15 nm in height. For an accurate calculation, small elements are required for a better approximation of the geometry. Nevertheless, the computing time is lengthened, and a compromise may be found. In the present work, the mode extraction was carried out with approximately 14 000 tetrahedrals. We have checked that increasing the number of elements produces a shift of eigenfrequency values smaller than the experimental resolution. In the end, the mass and stiffness matrices of the complete structure are computed, and give access to vibration modes.

For a gold dot on silicon, the mismatch of the acoustical impedances (of around 72%) is very large. Consequently, the lifetimes of the nanostructure vibrational modes should be large [see Fig. 3(b)] since the acoustic energy is expected to leak slowly into the silicon substrate. In that case, the dot may be reasonably described as an isolated system. Thus, the dot

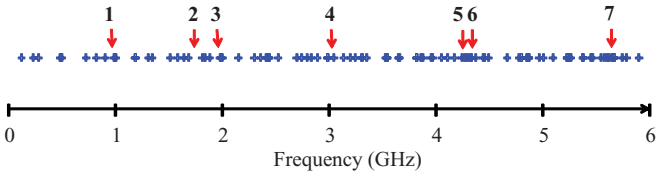

FIG. 5. (Color online) The blue crosses represent the calculated eigenmodes of vibration. Gold mechanical parameters used in the simulations are the following: density 19 300 kg/m^3, Young's modulus 78 GPa, and Poisson's ratio 0.44. Red arrows correspond to the first seven specific modes, which can be detected accordingly to the detection rules of our interferometric setup.

eigenmodes have been calculated here including free boundary conditions at all the dot interfaces. Nevertheless, the simulated response, displayed in Fig. 5, is obviously more complex than the experimental one: the dot exhibits a larger number of eigenmodes within the same frequency range. Therefore, we need to take into account the detection rule related to the interferometric scheme used in our picosecond experiments.

Similar reflectivity experiments performed on the single Au dot show no oscillation signature. Consequently, the photoelastic mechanism could be neglected, and then the only relevant quantity in Eq. (1) is the dot surface displacement perpendicular to the surface. To calculate the detectable signal of each vibrational mode in the experimental spectrum, a modulation of the dot displacement by a Gaussian probe intensity profile has been carried out using the following equation:

$$\frac{\Delta r\,(t)}{r_0} \alpha \int_0^{2\pi} \int_0^{D/2} u_s\,(r,\theta)\, \exp\left(-\frac{8r^2}{d^2}\right) r\,dr\,d\theta \qquad (3)$$

with u_s the normal dot surface displacement, D the dot diameter, and d the size of the probe spot (here 0.75 μm)

As a direct and obvious consequence, the vibrational modes dominated by in-plane strain give no detectable signal. In Fig. 5, we have pointed out (up to 5.3 GHz) the vibrational modes that give a signal according to our detection scheme. In very good agreement with the experimental spectrum of the dot, seven typical frequencies can be observed around 0.9, 1.7, 1.9, 3, 4.2, 4.3, and 5.6 GHz. The normal surface displacement component of the vibrational modes that are detected is displayed in Fig. 6. It appears very clearly that the symmetry of these modes follows the axial energy distribution of the pump beam.

Finally, to investigate the dot dimension effect on the frequency resonance, a set of experiments and calculations with different dimensions has been performed. Table I presents the experimental frequency detected and the first detectable modes, presented in Fig. 6, in accordance with the detection (3). An excellent agreement between theoretical and experimental data is obtained, even though changes in dot dimensions are tiny. The small deviations can be ascribed to the previous observable roughness of the dot. For example, a fluctuation of 20 nm on a 0.3-μm-diam dot modified the frequency position of the acoustic modes by 5%–10%. One can also notice that some modes are missing in the experimental spectrum, probably due to the finite lifetimes of the vibrations, which broaden the experimental peaks and the excitation

TABLE I. Comparison between simulated and experimental vibration modes for different dimensions of the gold dot.

Dots characteristics	Experiment (GHz)	Simulation (GHz)
Au	0.85	0.90
Diameter = 0.9 μm	1.35	1.69
Thickness = 55 nm	1.74	1.88
	2	3
	2.89	4.25
	4	4.32
	5.18	5.65
Au	0.83	1.03
Diameter = 0.7 μm	1.47	2.09
Thickness = 175 nm	2.63	2.72
	3.81	4.02
	4.65	4.40
	5.44	4.90
		5.36
Au	1.17	0.82
Diameter = 0.5 μm	3.28	2.70
Thickness = 55 nm	5.12	3.02
	6.92	5.01
		7.40
Au	1.23	1.96
Diameter = 0.3 μm	5.08	4.96
Thickness = 55 nm	9.53	5.79
	11.25	9.66
		11.42

processes. The excitation processes play also a major role in the vibrational landscape of a nanostructure. For example, it cannot be expected that modes of vibration exhibiting a complex pattern of deformation without the axial symmetry can be efficiently excited with a Gaussian. Moreover, if Eq. (3) is applied on such distributions, the predicted signal is close to zero. Therefore, in the case presented in this paper, both the excitation and the detection process should be taken into account to explain why only the specific modes shown in Fig. 6 can be observed.

Whereas vibrational modes with out-of-plane displacements have only been revealed in picosecond acoustic

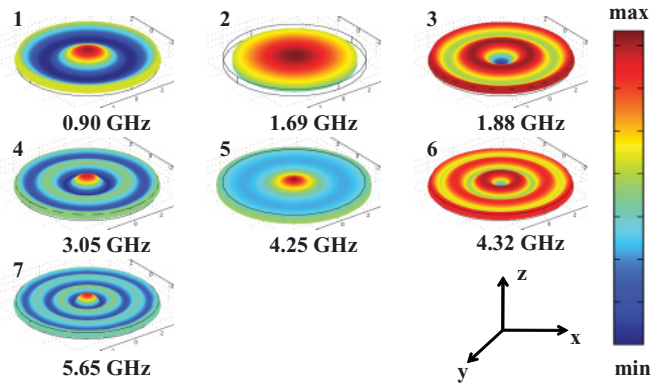

FIG. 6. (Color online) Mapping of the surface displacement of detectable vibrational modes. The color scale represents the displacement of the dot surface in the z direction.

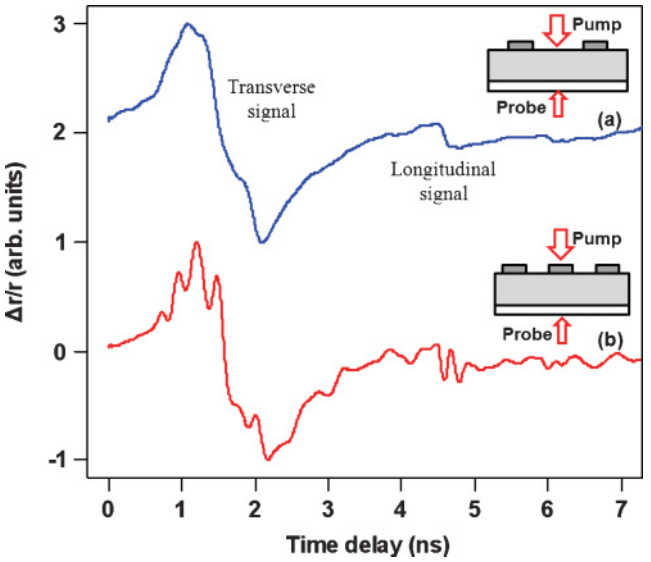

FIG. 7. (Color online) (a) Time-resolved signal obtained for a pump excitation located between the gold dot. (b) Time-resolved signal obtained for a pump localized on a single gold dot. An additional signal, traveling across the silicon substrate at the transverse velocity, is clearly visible.

measurements, the vibrational landscape presented in Fig. 5 suggests that more complex modes including in-plane dot modes may be excited. The dots are only weakly bonded to the substrate, as previously suggested by their experimental vibrational spectrum, but nevertheless some acoustic energy leaks into the substrate and the dot may act as a generator, even if the transduction efficiency may be increased with a better matching between the dot and the substrate. The last part of this paper is focused on the transduction properties of such gold nanostructures into the substrate.

B. Generation of tunable transverse bulk waves

To investigate the transduction properties of the gold nanostructures, experiments in the back side configuration have been performed. Here, the pump is focused on the side where the nanostructure array has been patterned, whereas the probe recorded the acoustic response through the change in reflectivity of an aluminum layer (100 nm) deposited on the opposite side. Figure 7 displays the time-resolved signal detected with a probe fixed at the pump epicentre. The time origin was arbitrarily taken just before the broad dipolar signal.

The upper curve displays the signal detected when the pump beam is localized between the dots. First we detected a broad structure and around 4 ns after a small kick is revealed. It is well known that phonon propagation in anisotropic systems gives rise to specific properties. In particular, quasitransverse and quasilongitudinal waves exist with different phase velocities and energy distributions. Such behavior has been intensively studied in the so-called phonon focusing phenomenon.[35] Recently, picosecond experiments have revealed similar results with high-frequency coherent waves in Si.[36] In the present case of a transmission experiment on a very thick substrate, the traveling time of both transverse and longitudinal waves is larger than the laser repetition time, but the acoustic signal

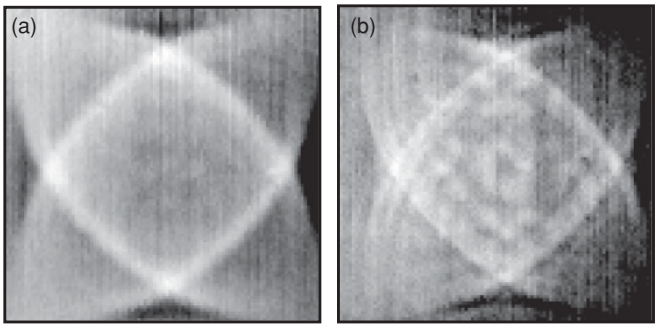

FIG. 8. 73×73 μm^2 surface displacement mapping. (a) The pump beam is located between the dot. (b) Additive acoustic feature induced when the pump beam has an individual gold dot with a diameter of 1.1 μm.

can be detected by a probe pulse emitted after the pulse of generation; therefore any acoustic event is folded back in a time window of 12.5 ns, which explains why a transverse signal may be detected before a longitudinal one. Taking into account the sound velocity of the transverse (5.8 nm/ps in [100]) and longitudinal (8.4 nn/ps in [100]) waves, the silicon thickness, and the laser repetition rate, the time separation between these acoustic signatures is estimated to be 4 ns, in very good agreement with experimental results. As the pump is focused on a single gold dot, an additional oscillatory signal is observed [see Fig. 7(b)], starting at the same time as the transverse signal of the silicon. To demonstrate conclusively that this additional signal, coming from the dot excitation, presents a transverse polarization, acoustic mapping has been done around the pump epicenter. A typical snapshot of the sample displacement is presented in Fig. 8. The signal detected with a pump besides the dot is presented in Fig. 8(a). Solving the Christoffel equation for a silicon cubic lattice, such a wave front imaging may be clearly ascribed to the propagation of a slow transverse wave; for details, see Ref. 36. The distribution

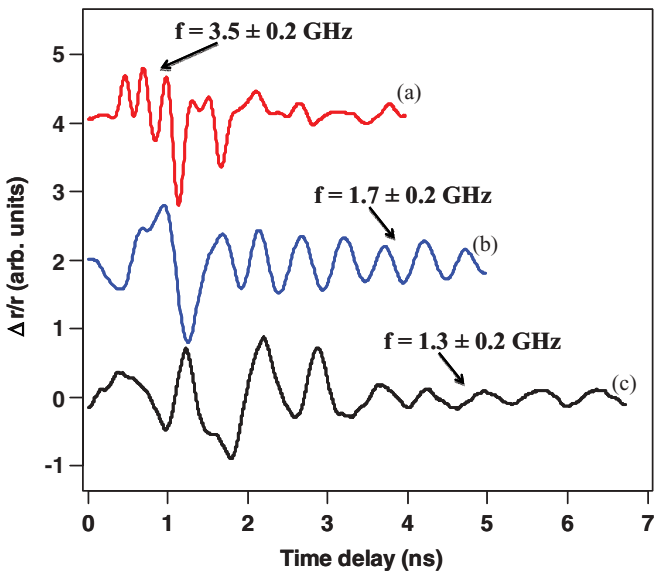

FIG. 9. (Color online) Transverse generation signal associated with a dot with different diameters: (a) $d = 0.5$ μm, (b) $d = 0.9$ μm, and (c) $d = 1.1$ μm.

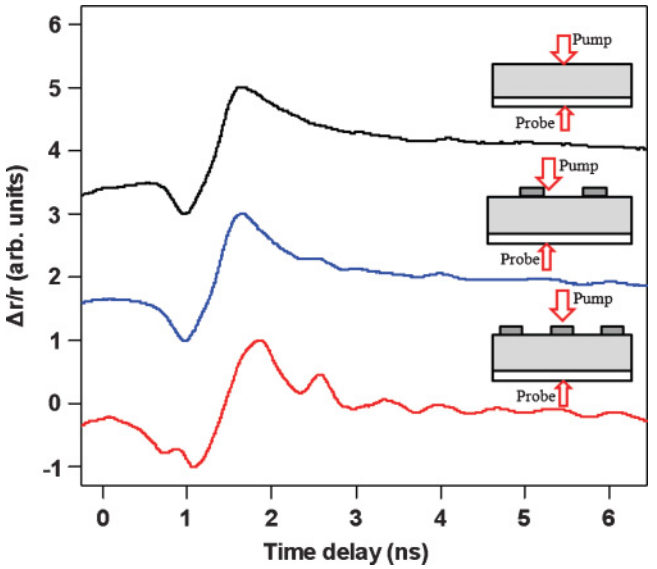

FIG. 10. (Color online) Transmission signal vs the position of the pump beam on the gold dot with $d = 1.1$ μm. We can notice a dot generation maximum when the pump is centered on the dot.

of the added diffracted signal coming from the dot [Fig. 8(b)] presents exactly the same symmetry, in good agreement with a slow transverse generation.

Moreover, we emphasize that the frequency spectrum of this additional signal depends on the dot diameter, as shown in Fig. 9. The main frequencies detected for gold dot with respective diameters of 1.1, 0.9, and 0.5 μm are 1.3 ± 0.2, 1.7 ± 0.2, and 3.5 ± 0.2 GHz, respectively. Finally, in Fig. 10, the generation efficiency is investigated in terms of the position of the pump beam over the gold dot with a fixed probe position. We observed a maximum of the transverse generation when the pump is located right in the center of the dot.

Now to determine the mode that emits such transverse waves, the dot displacements in the plane parallel to the substrate surface must be considered. Among all the previous simulated eigenmodes presented in Fig. 5 (blue crosses), the best candidate is the vibrational mode described in Fig. 11, exhibiting the larger in-plane displacement. The frequency of this first breathing mode has been calculated for different dot sizes, as shown in Fig. 12. The dependence of the

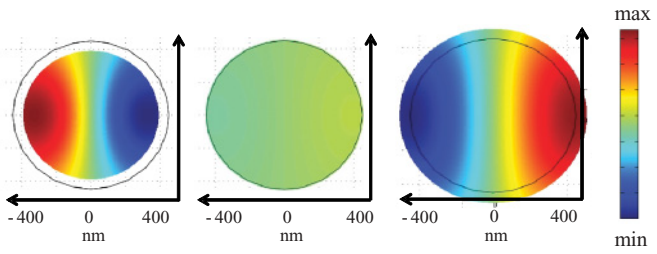

FIG. 11. (Color online) Displacement mapping in the x direction calculated for a 0.9-μm-diam dot at different time delay. The separation time is equal to 0.59 ns. The frequency of this vibration mode is located at 1.69 GHz. The black circle represents the initial dot diameter. The maximal in-plane displacement may be estimated at 57 nm.

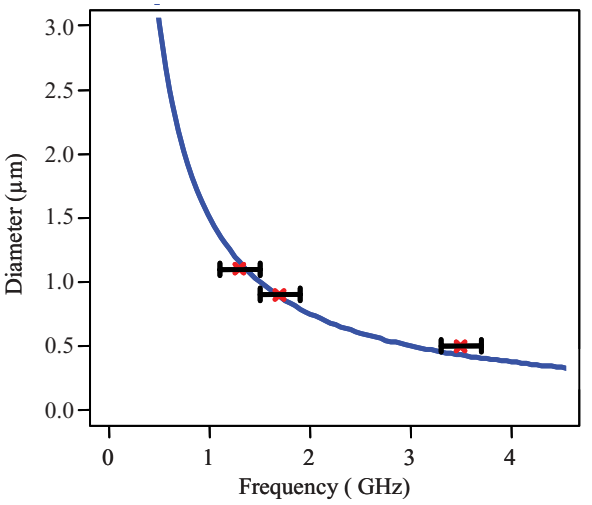

FIG. 12. (Color online) Evolution of the frequency of the transverse wave generation vs the dot diameter. The experimental frequencies, marked with red crosses, follow a $1/D$ law.

frequency versus the dot diameter follows a $1/D$ law without any influence of the thickness for the dots studied here.[37] We can notice a good agreement between the simulations and the experimental frequencies. Therefore, transverse waves with tunable frequency can be obtained by changing the geometric parameters of the dots. So using such lithographed dots, transverse waves can be excited without any constraint link to the elasticity, the orientation, or the anisotropy of the system under study.

IV. CONCLUSIONS

In this paper, we have detailed our investigation of the vibrational behavior of lithographed gold structures. Mixing 3D finite-element simulations and experimental detection rules, the experimental vibrational spectrum in the gold structures is reproduced with good accuracy. It is shown that acoustic resonances at frequency up to 11 GHz can be excited, a value that could be even higher if smaller or harder structures could be efficiently excited. Finally, using acoustic transmission measurements, we clearly evidenced that such lithographed structures may be good candidates for an efficient transduction of bulk transverse waves. Using dots with different diameters, we illustrate the possibility to tune the frequency of this acoustic emission.

In the near future, by arranging the distribution of these acoustic sources and controlling their size, we might consider creating specific acoustic patterning including a frequency control, as has already be done in the ondulatory optical field, or in medical ultrasonics at a lower frequency range. High-frequency transverse wave generation opens a large field of applications, such as measurements of stiffness or transverse viscosity, the study of solid-liquid phase transitions,[38] or high-speed tribology.

ACKNOWLEDGMENT

This work has been supported by ANR Contract No. ANR-08-BLAN-0109-01.

*Author to whom all correspondence should be addressed: laurent.belliard@upmc.fr

[1]N. Del Fatti, C. Voisin, F. Chevy, F. Vallée, and C. Flytzanis, J. Chem. Phys. **110**, 11484 (1999).
[2]G. Piazza, J. Stephanou, and P. A. Pisano, J. Microelectromech. Syst. **15**, 1406 (2006).
[3]M. A. van Dijk, M. Lippitz, and M. Orrit, Phys. Rev. Lett. **95**, 267406 (2005).
[4]C. Thomsen, J. Strait, Z. Vardeny, H. J. Maris, J. Tauc, and J. J. Hauser, Phys. Rev. Lett. **53**, 989 (1984).
[5]C. Thomsen, H. T. Grahn, H. J. Maris, and J. Tauc, Phys. Rev. B **34**, 4129 (1986).
[6]W. Chen, Y. Lu, H. J. Maris, and G. Xiao, Phys. Rev. B **50**, 14506 (1994).
[7]N. W. Pu, J. Bokor, S. Jeong, and R.-I. Zhao, Appl. Phys. Lett. **74**, 320 (1999).
[8]L. Belliard, A. Huynh, B. Perrin, A. Michel, G. Abadias, and C. Jaouen, Phys. Rev. B **80**, 155424 (2009).
[9]A. Vertikov, M. Kuball, A. V. Nurmikko, and H. J. Maris, Appl. Phys. Lett. **69**, 2465 (1996).
[10]P. Siry, L. Belliard, and B. Perrin, Acta Acustica. **89**, 925 (2003).
[11]Y. Guillet, C. Rossignol, B. Audoin, G. Calbris, and S. Ravaine, Appl. Phys. Lett. **95**, 061909 (2009).
[12]C. Coupeau, P. Goudeau, L. Belliard, M. George, N. Tamura, F. Cleymand, J. Colin, B. Perrin, and J. Grilhé, Thin Solid Films **469-470**, 221 (2004).
[13]Y. Sugawara, O. B. Wright, O. Matsuda, M. Takigahira, Y. Tanaka, S. Tamura, and V. E. Gusev, Phys. Rev. Lett. **88**, 185504 (2002).
[14]D. M. Profunser, E. Muramoto, O. Matsuda, O. B. Wright, and U. Lang, Phys. Rev. B **80**, 014301 (2009).
[15]T. Dehoux, N. Chigarev, C. Rossignol, and B. Audoin, Phys. Rev. B **77**, 214307 (2008).
[16]D. H. Hurley, O. B. Wright, O. Matsuda, V. E. Gusev, and O. V. Kolosov, Ultrasonics **38**, 470 (2000).
[17]T. Pezeril, P. Ruello, S. Gougeon, N. Chigarev, D. Mounier, J.-M. Breteau, P. Picart, and V. Gusev, Phys. Rev. B **75**, 174307 (2007).
[18]V. Gusev, J. Appl. Phys. **107**, 114906 (2010).
[19]V. Gusev, Appl. Phys. Lett. **94**, 164105 (2009).
[20]C. Rossignol, J. M. Rampnoux, M. Perton, B. Audoin, and S. Dilhaire, Phys. Rev. Lett. **94**, 166106 (2005).
[21]B. Bonello, A. Ajinou, V. Richard, P. Djemia, and S. M. Cherif, J. Acoust. Soc. Am. **110**, 1943 (2001).
[22]D. Hurley, Appl. Rev. Lett. **88**, 191106 (2006).
[23]H. T. Grahn, H. J. Maris, J. Tauc, and B. Abeles, Phys. Rev. B **38**, 6066 (1988).
[24]B. Perrin, B. Bonello, J. C. Jeannet, and E. Romatet, Prog. Nat. Sci. **S6**, 444 (1996).
[25]O. B. Wright and T. Hyoguchi, Opt. Lett. **16**, 1529 (1991).
[26]B. Perrin, C. Rossignol, B. Bonello, and J.-C. Jeannet, Physica B **263-264**, 571 (1999).
[27]Y. Sugawara, O. B. Wright, O. Matsuda, and V. E. Gusev, Ultrasonics **40**, 55 (2002).
[28]C. Rossignol, B. Perrin, S. Laborde, L. Vandenbulcke, M. I. Barros, and P. Djemia, J. Appl. Phys. **95**, 4157 (2004).
[29]G. A. Antonelli, B. Perrin, B. C. Daly, and D. G. Cahill, MRS Bull. **31**, 607 (2006).
[30]T. Bienville, J.-F. Robillard, L. Belliard, I. Roch-Jeune, A. Devos, and B. Perrin, Ultrasonics **44**, e1289 (2006).
[31]T. Bienville, L. Belliard, P. Siry, and B. Perrin, Superlatt. Microstruct. **35**, 363 (2004).
[32]F. Decremps, L. Belliard, B. Perrin, and M. Gauthier, Phys. Rev. Lett. **100**, 035502 (2008).
[33]D. R. Lide, *CRC Handbook of Chemistry and Physics*, 79th ed. (CRC, Boca Raton, FL, 1999).
[34]J. F. Ready, *Effects of High-Power Laser Radiation* (Academic, New York, 1971).
[35]A. G. Every, W. Sachse, K. Y. Kim, and M. O. Thompson, Phys. Rev. Lett. **65**, 1446 (1990).
[36]F. Decremps, L. Belliard, M. Gauthier, and B. Perrin, Phys. Rev. B **82**, 104119 (2010).
[37]D. C. Gazis, J. Acoust. Soc. Am. **31,** 568 (1959); **30**, 786 (1958)
[38]F. Decremps, L. Belliard, B. Couzinet, S. Vincent, P. Munsch, G. Le Marchand, and B. Perrin, Rev. Sci. Instrum. **80**, 073902 (2009).